Lattice-Boltzmann modeling of phonon hydrodynamics

Wen-Shu Jiaung* and Jeng-Rong Ho†
Department of Mechanical Engineering, National Chung Cheng University, Ming-Hsiung, Chia-Yi 621 Taiwan, Republic of China
(Received 2 November 2007; published 23 June 2008)

Based on the phonon Boltzmann equation, a lattice-Boltzmann model for phonon hydrodynamics is developed. Both transverse and longitudinal polarized phonons that interact through normal and umklapp processes are considered in the model. The collision term is approximated by the relaxation time model where normal and umklapp processes tend to relax distributions of phonons to their corresponding equilibrium distribution functions—the displaced Planck distribution and the Planck distribution, respectively. A macroscopic phonon thermal wave equation (PTWE), valid for the second-sound mode, is derived through the technique of Chapman-Enskog expansion. Compared to the dual-phase-lag (DPL) -based thermal wave equation, the PTWE has an additional fourth-ordered spatial derivative term. The fundamental difference between the two models is discussed through examining a propagating thermal pulse in a single-phased medium and the transient and steady-state transport phenomena on a two-layered structure subjected to different temperatures at boundaries. Results show that transport phenomena are significantly different between the two models. The behavior exhibited by the DPL model, as thermal wave behavior goes over to diffusive behavior, $\tau_T \rightarrow \tau_q$ is incompatible with any microscopic phonon propagating mode. Unlike the DPL model, in which τ_T only has an effect on the transient phenomena, in the PTWE model τ_T shows effects on phenomena at both transient and steady state. With the intrinsic compatibility to the microscopic state, discontinuous quantities, such as a jump of temperature at a boundary or at an interface, can be calculated naturally and straightforwardly with the present lattice-Boltzmann method.

DOI: 10.1103/PhysRevE.77.066710 PACS number(s): 05.10.−a, 44.90.+c, 63.20.−e

I. INTRODUCTION

The transport of heat described by Fourier's law has been demonstrated to give rise to unreasonable results in several situations. The anomaly is due to the assumption that the heat flux vector and the temperature gradient occur at the same instant of time; this leads to an infinite speed of heat propagation [1]. Cattaneo [2] and Vernotte [3] proposed a relaxation model to resolve this dilemma that results in the wave-based hyperbolic heat conduction equation. A comprehensive literature survey of thermal waves can be found in the review papers by Joseph and Preziosi [4,5] and by Ozisik and Tzou [6]. Although the CVW (wave model proposed by Cattaneo and Vernotte) remedies the paradox of the instantaneous response of thermal disturbance, it also introduces some unusual solutions [7,8].

Instead of the precedence assumption of the lead of the temperature gradient to the heat flux, Tzou proposed a dual-phase-lag (DPL) model that allows either the temperature gradient to precede the heat flux or the heat flux to precede the temperature gradient [9–11]. The heat conduction equation based on the DPL model is given by

$$\hat{\tau}_q \frac{\partial^2 \hat{\theta}}{\partial \hat{t}^2} + \frac{\partial \hat{\theta}}{\partial \hat{t}} = \hat{\alpha} \frac{\partial^2 \hat{\theta}}{\partial \hat{\mathbf{x}}^2} + \hat{\alpha} \hat{\tau}_T \frac{\partial^3 \hat{\theta}}{\partial \hat{\mathbf{x}}^2 \partial \hat{t}}, \tag{1}$$

where $\hat{\tau}_q$ represents the phase-lag time between the temperature gradient and the commencement of heat flow while $\hat{\tau}_T$ is the lag of the temperature gradient to the heat flow. This model can reduce to diffusion, CVW, the phonon-electron interaction, and the pure phonon scattering models under suitable values of $\hat{\tau}_q$ and $\hat{\tau}_T$. It thus can cover a wide range of physical responses from microscopic to macroscopic scales in both space and time. More recent research interests based on the DPL model are summarized in our previous work of lattice-Boltzmann modeling for the DPL-based heat conduction equation [12].

The above review quickly portrays models for heat transport from the macroscopic approach. Microscopically, transport of energy in a dielectric solid is accomplished through atomic vibrations that travel within the solid as waves. The interatomic coupling present in a solid allows many different vibrational modes that correspond to waves with different frequencies. Just as the energy of an electromagnetic wave is quantized, the energy of the waves can be quantized as phonons and the solid medium can be treated as phonon gas. The Boltzmann equation (Boltzmann-Peierls equation) is one of the tools that is often used in the description of phonon interactions, such as modeling for lattice thermal conductivity, phenomena of the second sound, and the Poiseuille flow [13–19]. Depending on the relative strength of the normal processes and resistive processes, the phonon propagation can be classified as the following modes: ballistics, diffusion, second sound, and heat conduction. These modes can be further separated into two groups as the individual propagation modes that include the ballistics and diffusion modes as well as the collective propagation modes which cover the second sound, and heat conduction modes [20].

Thermal wave is the collective (or hydrodynamic) behavior of the interacting phonon system that fits in the second-

*Researcher, Mechanical & Systems Research Laboratories, Industrial Technology Research Institute, Hsin-Chu, Taiwan, Republic of China.
†Author to whom correspondence should be addressed; FAX: +886-5-2720589; imerjrho@ccu.edu.tw

sound mode in which the normal processes strongly predominate. To study the nonlinear phonon hydrodynamic behaviors, Guyer proposed a lattice-Boltzmann scheme to model the phonon gas [21]. In this model, both transverse and longitudinal types of phonons that interact with one another through a three-phonon collision process were performed on a two-dimensional hexagonal, the D2Q7 lattices. Although several nonlinear phonon behaviors that were beyond description of the linearized phonon hydrodynamics were successfully demonstrated, only the momentum conserving processes, the normal processes (N processes), were considered in this study. Most recently, Amon *et al.* employed the LBM to model the Boltzmann transport equation of phonons for the simulation of conduction of heat for both crystalline and amorphous materials at different time and length scales. They demonstrated the transition of energy transport from the regimes of diffusive to ballistic could be well addressed by the phonon LBM model [22–24].

Motivated by connecting the microscopic phonon interaction modes to their corresponding macroscopic heat transfer behaviors, the present study examines the heat conduction equation from the phonon Boltzmann equation. Since N processes alone cannot lead to finite heat conductivity, the umklapp processes (U processes) are included in the present model as well. The connection between the phonon Boltzmann equation and the macroscopic heat conduction equation is established through the technique of the Chapman-Enskog multiscale expansion. The obtained heat conduction equation is then compared with the DPL-based heat conduction equation, Eq. (1). The fundamental difference between these two equations is discussed through two illustrative examples that concern propagating a heat pulse in a single-phased medium and transient and steady-state transport phenomena within a two-layered thin film structure subjected to different temperatures at two boundaries.

II. LATTICE-BOLTZMANN MODELING FOR PHONON GAS

In order to describe transport of heat, we consider the wave packets of phonons of polarization σ and group velocity $\hat{\mathbf{c}}^{\sigma}$ that can be localized in regions smaller than a characteristic wavelength of the external thermal perturbation. All interesting physical quantities can be obtained provided the distribution functions $\hat{f}^{\sigma}(\hat{t},\hat{\mathbf{x}},\hat{\mathbf{c}})$ of phonons at position $\hat{\mathbf{x}}$ and time $\hat{t}$ are known. The evolution of $\hat{f}^{\sigma}(\hat{t},\hat{\mathbf{x}},\hat{\mathbf{c}})$ is assumed to obey the Boltzmann equation

$$\frac{\partial \hat{f}^{\sigma}}{\partial \hat{t}} + \hat{\mathbf{c}}^{\sigma}\hat{\nabla}\hat{f}^{\sigma} = \left(\frac{\delta \hat{f}^{\sigma}}{\delta t}\right)_N + \left(\frac{\delta \hat{f}^{\sigma}}{\delta t}\right)_R. \tag{2}$$

The right-hand side of Eq. (2) represents contributions from collisions where the first term comprises the normal processes and the second term is the resistive part that includes umklapp processes, impurity scattering, and boundary scattering. In the present study, all such momentum-destroying processes are designated as the U processes, thus $(\delta \hat{f}^{\sigma}/\delta t)_R$ is expressed as $(\delta \hat{f}^{\sigma}/\delta t)_U$.

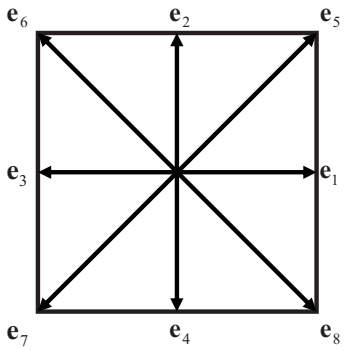

$$\begin{array}{llll}
\mathbf{e}_1=(1,0) & \mathbf{c}_1^{\sigma}=(1+\sigma)\mathbf{e}_1 & \epsilon_1^{\sigma}=(1+\sigma)\epsilon & \mathbf{p}_1^{\sigma}=p\mathbf{e}_1 \\
\mathbf{e}_2=(0,1) & \mathbf{c}_2^{\sigma}=(1+\sigma)\mathbf{e}_2 & \epsilon_2^{\sigma}=(1+\sigma)\epsilon & \mathbf{p}_2^{\sigma}=p\mathbf{e}_2 \\
\mathbf{e}_3=(-1,0) & \mathbf{c}_3^{\sigma}=(1+\sigma)\mathbf{e}_3 & \epsilon_3^{\sigma}=(1+\sigma)\epsilon & \mathbf{p}_3^{\sigma}=p\mathbf{e}_3 \\
\mathbf{e}_4=(0,-1) & \mathbf{c}_4^{\sigma}=(1+\sigma)\mathbf{e}_4 & \epsilon_4^{\sigma}=(1+\sigma)\epsilon & \mathbf{p}_4^{\sigma}=p\mathbf{e}_4 \\
\mathbf{e}_5=(1,1) & \mathbf{c}_5^{\sigma}=(1+\sigma)\mathbf{e}_5 & \epsilon_5^{\sigma}=2(1+\sigma)\epsilon & \mathbf{p}_5^{\sigma}=p\mathbf{e}_5 \\
\mathbf{e}_6=(-1,1) & \mathbf{c}_6^{\sigma}=(1+\sigma)\mathbf{e}_6 & \epsilon_6^{\sigma}=2(1+\sigma)\epsilon & \mathbf{p}_6^{\sigma}=p\mathbf{e}_6 \\
\mathbf{e}_7=(-1,-1) & \mathbf{c}_7^{\sigma}=(1+\sigma)\mathbf{e}_7 & \epsilon_7^{\sigma}=2(1+\sigma)\epsilon & \mathbf{p}_7^{\sigma}=p\mathbf{e}_7 \\
\mathbf{e}_8=(1,-1) & \mathbf{c}_8^{\sigma}=(1+\sigma)\mathbf{e}_8 & \epsilon_8^{\sigma}=2(1+\sigma)\epsilon & \mathbf{p}_8^{\sigma}=p\mathbf{e}_8
\end{array}$$

FIG. 1. Schematic diagram showing the D2Q9 lattice. There are eight directions, designated as $\mathbf{e}_i$, $i=1,2,\ldots,8$, in each lattice. The direction $\mathbf{e}_0$ with zero phonon velocity is not considered. Polarized phonon direction velocity $\mathbf{c}_i^{\sigma}$, energy ϵ_i^{σ}, and momentum $\mathbf{p}_i^{\sigma}$ in each direction are listed. $\sigma=0$ and 1 represent transverse and longitudinal phonons, respectively. c and ϵ denote the unit speed and unit energy.

A. *Lattice-Boltzmann equation for phonons*

The treatment of the collision term is based on the relaxation time approximation. Equation (2) is expressed as

$$\frac{\partial \hat{f}^{\sigma}}{\partial \hat{t}} + \hat{\mathbf{c}}^{\sigma}\hat{\nabla}\hat{f}^{\sigma} = -\frac{1}{\hat{\tau}_N}(\hat{f}^{\sigma}-\hat{f}^{\sigma(0)}) - \frac{1}{\hat{\tau}_U}(\hat{f}^{\sigma}-\hat{f}_0^{\sigma(0)}), \tag{3}$$

where the equilibrium distribution functions $\hat{f}^{\sigma(0)}$ and $\hat{f}_0^{\sigma(0)}$ represent the displaced Planck distribution and Planck distribution, respectively. The U processes tend to return the phonon system to an equilibrium Planck distribution, whereas the N processes relax to a displaced Planck distribution [13]. $\hat{\tau}_N$ and $\hat{\tau}_U$ are the relaxation times for the normal and umklapp processes. The phonon Boltzmann equation will be nondimensionalized by the characteristic length scale $\hat{L}$, velocity scale $\hat{U}$, energy scale $\hat{\Theta}$, time between collisions $\hat{t}_c$, and the reference density distribution functions $\hat{f}_R$, as

$$\frac{\partial f^{\sigma}}{\partial t} + \mathbf{c}^{\sigma}\nabla f^{\sigma} = -\frac{1}{\varepsilon\tau_N}(f^{\sigma}-f^{\sigma(0)}) - \frac{1}{\varepsilon\tau_U}(f^{\sigma}-f_0^{\sigma(0)}), \tag{4}$$

where $\mathbf{c}^{\sigma}=\hat{\mathbf{c}}^{\sigma}/\hat{U}$, $\nabla=\hat{L}\hat{\nabla}$, $t=\hat{t}\hat{U}/\hat{L}$, $\tau_{N,U}=\hat{\tau}_{N,U}/\hat{t}_c$, and $\varepsilon=\hat{t}_c\hat{U}/\hat{L}$.

A two-dimensional physical space that consists of D2Q9 lattices is used in this study. As shown in Fig. 1, there are

eight directions, designed as $\mathbf{e}_i$, $i=1,\ldots,8$, on each lattice. Due to the zero phonon speed, the direction of $\mathbf{e}_0$ is not considered. Both the thermal excited phonon polarization, transverse and longitudinal phonons denoted, respectively, as $\sigma=0$ and 1, are considered. Hence, at each site there are 16 phonon states including eight transverse states and eight longitudinal states. At each state phonons propagate with velocity $\mathbf{c}_i^\sigma = c^\sigma \mathbf{e}_i$, where $c^\sigma=(1+\sigma)c$ and c is the magnitude of unit speed. The energy at each state, ϵ_i^σ, is set as $\epsilon_i^\sigma = (1+\sigma)\epsilon$ for phonons in directions $\mathbf{e}_i$, $i=1,2,3,4$, and $\epsilon_i^\sigma = 2(1+\sigma)\epsilon$ for directions $\mathbf{e}_i$, $i=5,6,7,8$. In these expressions, ϵ denotes the amount of unit energy. The phonon momentum on each polarization is denoted as $\mathbf{p}_i^\sigma = p\mathbf{e}_i$, where we assume the relation for phonon energy and phonon momentum follows $\epsilon_i^\sigma = \mathbf{p}_i^\sigma \cdot \mathbf{c}_i^\sigma$, the regime where the Debye model is appropriate. The amount of unit momentum is thus given as $p = \epsilon/c$.

A discretization of Eq. (4) leads to the lattice-Boltzmann equation for phonon gas (see Appendix A for the details),

$$f_i^\sigma(\mathbf{x}+c^\sigma \mathbf{e}_i \Delta t, t+\Delta t) - f_i^\sigma(\mathbf{x},t) = -\frac{1}{\tau_N}(f_i^\sigma - f_i^{\sigma(0)}) - \frac{1}{\tau_U}(f_i^\sigma - f_{0,i}^{\sigma(0)}). \tag{5}$$

Define a combined relaxation time τ_C as $1/\tau_C \equiv 1/\tau_N + 1/\tau_U$. Equation (5) can be written as

$$f_i^\sigma(\mathbf{x}+c^\sigma \mathbf{e}_i \Delta t, t+\Delta t) - f_i^\sigma(\mathbf{x},t) = -\frac{1}{\tau_C}(f_i^\sigma - f_i^{\sigma(0)}) - \frac{1}{\tau_U}(f_i^{\sigma(0)} - f_{0,i}^{\sigma(0)}). \tag{6}$$

B. *Equilibrium distribution functions*

N processes conserve momentum and lead to the weighted displaced Planck distribution function in the direction i as

$$f_i^{\sigma(0)} = \frac{w_i^\sigma}{e^{\beta[\epsilon_i^\sigma - p\mathbf{e}_i\cdot\mathbf{u}]} - 1}, \tag{7}$$

where w_i^σ are the directional weights (see Appendix E), $\beta = 1/k_B T$, k_B is the Boltzmann constant, and $\mathbf{u}$ is the local drift velocity of the phonon gas. U processes relax phonons to the local equilibrium distribution, the Planck distribution. The weighted Planck distribution function for direction i is

$$f_{0,i}^{\sigma(0)} = \frac{w_i^\sigma}{e^{\beta\epsilon_i^\sigma} - 1}. \tag{8}$$

The Planck distribution function is thus a special case of the displaced Planck distribution function when the phonon drift velocity $\mathbf{u}$ is zero.

When the medium, initially at equilibrium at temperature T_0 with the drift velocity $\mathbf{u}_0=0$, is subjected to a thermal disturbance, a disturbed drift velocity $\mathbf{u}=\mathbf{u}_0+\delta\mathbf{u}$ is initiated, and the displaced Planck distribution function can be written as

$$f_i^{\sigma(0)} = \frac{w_i^\sigma}{\exp\left[\beta_0\epsilon_i^\sigma(1-\theta) - \beta_0\epsilon\mathbf{e}_i\cdot\frac{\delta\mathbf{u}}{c}(1-\theta)\right] - 1},$$

or, more compactly, as

$$f_i^{\sigma(0)} = \frac{w_i^\sigma}{\exp[\beta_0\epsilon_i^\sigma(1-\theta) - \beta_0\epsilon\mathbf{e}_i\cdot\mathbf{v}(1-\theta)] - 1}, \tag{9}$$

where $\mathbf{v}$ is the normalized disturbed drift velocity, defined as $\mathbf{v}=\delta\mathbf{u}/c$, and θ is the perturbed temperature, $\theta=(\beta_0-\beta)/\beta_0$. Here $\beta_0 = 1/k_B T_0$. θ can also be expressed as $\theta = \delta T/T$, where δT is the amount of temperature perturbation with respect to the equilibrium temperature T_0.

Define the directional equilibrium distribution function for medium at $\mathbf{v}=0$ and $\theta=0$ as

$$\bar{f}_{0,i}^{\sigma(0)} = [\exp(\beta_0\epsilon_i^\sigma) - 1]^{-1}, \tag{10}$$

and expanding Eq. (7) based on Eq. (10) yields

$$f_i^{\sigma(0)} = w_i^\sigma[\bar{f}_{0,i}^{\sigma(0)} - \bar{f}_{0,i}'^{\sigma(0)}\beta_0\epsilon_i^\sigma\theta - \bar{f}_{0,i}'^{\sigma(0)}\beta_0\epsilon\mathbf{e}_i\cdot\mathbf{v} + O(\delta^2)], \tag{11}$$

where $O(\delta^2)$ represents the second-order perturbed terms, i.e., $O(\delta^2)=O(\theta^2,\theta\mathbf{v},\mathbf{v}\mathbf{v})$, $\bar{f}_{0,i}'^{\sigma(0)}$ is the first derivative of $\bar{f}_{0,i}^{\sigma(0)}$ with respect to $\beta_0\epsilon_i^\sigma$, and mathematically it can be proven that $\bar{f}_{0,i}'^{\sigma(0)} = -\bar{f}_{0,i}^{\sigma(0)}(1+\bar{f}_{0,i}^{\sigma(0)})$. Similarly, Eq. (8) can be expressed, based on Eq. (10), as $f_{0,i}^{\sigma(0)} = w_i^\sigma[\bar{f}_{0,i}^{\sigma(0)} - \beta_0\epsilon_i^\sigma\bar{f}_{0,i}'^{\sigma(0)}\theta]$, or

$$f_i^{\sigma(0)} = f_{0,i}^{\sigma(0)} - w_i^\sigma\bar{f}_{0,i}'^{\sigma(0)}\beta_0\epsilon\mathbf{e}_i\cdot\mathbf{v}. \tag{12}$$

The second term on the right-hand side is the effect contributed from the momentum disturbance, thus Eq. (12) indicates the displaced Planck distribution function can be approximated as the Planck distribution function plus the effect caused by the disturbance of the drift velocity. In the lattice-Boltzmann scheme, this term can be treated as an external force term [25]. The above distribution functions can be evaluated provided that θ and $\mathbf{v}$ are prescribed, which should be calculated from the energy and momentum equations.

The macroscopic physical quantities, energy density E, momentum density vector $\mathbf{P}$, heat flux vector $\mathbf{Q}$, and momentum flux tensor $B_{\alpha\beta}$, are averages through the phonon distribution functions that are given as

$$E = \sum_{i,\sigma} \epsilon_i^\sigma f_i^\sigma, \tag{13}$$

$$P_\alpha = \sum_{i,\sigma} p e_{i,\alpha} f_i^\sigma, \tag{14}$$

$$Q_\alpha = \sum_{i,\sigma} \epsilon_i^\sigma c^\sigma e_{i,\alpha} f_i^\sigma, \tag{15}$$

$$B_{\alpha\beta} = \sum_{i,\sigma} p e_{i,\alpha} c^\sigma e_{i,\beta} f_i^\sigma. \tag{16}$$

C. *Chapman-Enskog expansion*

Relations between the microscopic lattice-Boltzmann equation and the conservation laws that govern the macroscopic quantities can be established through the Chapman-Enskog expansion. In this expansion the particle distribution functions f_i^σ and $f_{0,i}^{\sigma(0)}$ are expanded with respect to the displaced Planck distribution function $f_i^{\sigma(0)}$, up to the second order of the expansion parameter ε as

$$f_i^\sigma = f_i^{\sigma(0)} + \varepsilon f_i^{\sigma(1)} + \varepsilon^2 f_i^{\sigma(2)} + O(\varepsilon^3), \tag{17}$$

and

$$f_{0,i}^{\sigma(0)} = f_i^{\sigma(0)} + \varepsilon f_{0,i}^{\sigma(1)} + \varepsilon^2 f_{0,i}^{\sigma(2)} + O(\varepsilon^3). \tag{18}$$

Comparing Eq. (18) with Eq. (12), we have $f_{0,i}^{\sigma(1)} = w_i^\sigma / \varepsilon[\beta_0 \varepsilon \bar{f}_{0,i}'^{\sigma(0)} \mathbf{e}_i \cdot \mathbf{v}]$ and $f_{0,i}^{\sigma(2)} = 0$. Substituting Eq. (17) into Eqs. (13)–(16), and separating the macroscopic quantities into two parts, the equilibrium part that is contributed by $f_i^{\sigma(0)}$, and the nonequilibrium part, which is caused mainly by the first-order term $f_i^{\sigma(1)}$, yields

$$E = E^{(\mathrm{eq})} + \varepsilon E^{(\mathrm{neq})} = \sum_{i,\sigma} \epsilon_i^\sigma f_i^{\sigma(0)} + \varepsilon \sum_{i,\sigma} \epsilon_i^\sigma f_i^{\sigma(1)}, \tag{19}$$

$$P_\alpha = P_\alpha^{(\mathrm{eq})} + \varepsilon P_\alpha^{(\mathrm{neq})} = \sum_{i,\sigma} p e_{i\alpha} f_i^{\sigma(0)} + \varepsilon \sum_{i,\sigma} p e_{i\alpha} f_i^{\sigma(1)}, \tag{20}$$

$$Q_\beta = Q_\beta^{(\mathrm{eq})} + \varepsilon Q_\beta^{(\mathrm{neq})} = \sum_{i,\sigma} \epsilon_i^\sigma c^\sigma e_{i\beta} f_i^{\sigma(0)} + \varepsilon \sum_{i,\sigma} \epsilon_i^\sigma c^\sigma e_{i\beta} f_i^{\sigma(1)}, \tag{21}$$

and

$$B_{\alpha\beta} = B_{\alpha\beta}^{(\mathrm{eq})} + \varepsilon B_{\alpha\beta}^{(\mathrm{neq})} = \sum_{i,\sigma} p e_{i\alpha} c^\sigma e_{i\beta} f_i^{\sigma(0)} + \varepsilon \sum_{i,\sigma} p e_{i\alpha} c^\sigma e_{i\beta} f_i^{\sigma(1)}. \tag{22}$$

The equilibrium portions of these macroscopic quantities can be obtained by substituting Eq. (9) into Eqs. (19)–(22) as

$$E^{(\mathrm{eq})} = \sum_{i,\sigma} \epsilon_i^\sigma f_i^{\sigma(0)} = E_0 + M_1 \theta, \tag{23}$$

$$P_\alpha^{(\mathrm{eq})} = \sum_{i,\sigma} p e_{i\alpha} f_i^{\sigma(0)} = p M_2 \delta_{\alpha\ell} v_\ell, \tag{24}$$

$$Q_\beta^{(\mathrm{eq})} = \sum_{i,\sigma} \epsilon_i^\sigma c^\sigma e_{i\beta} f_i^{\sigma(0)} = M_3 \delta_{\beta\ell} v_\ell, \tag{25}$$

and

$$B_{\alpha\beta}^{(\mathrm{eq})} = \sum_{i,\sigma} p e_{i\alpha} c^\sigma e_{i\beta} f_i^{\sigma(0)} = B_0 \delta_{\alpha\beta} + \frac{p}{\epsilon} M_3 \delta_{\alpha\beta} \theta, \tag{26}$$

where the coefficients M_1, M_2, and M_3 are presented in Appendix B. These expressions only relate the equilibrium macroscopic quantities to temperature and velocity variations. To obtain the nonequilibrium parts, the function of $f_i^{\sigma(1)}$ should be calculated.

The expansion of $f_i^\sigma(\mathbf{x} + c_i^\sigma \mathbf{e}_i \Delta t, t + \Delta t)$ up to $O(\Delta t^2)$ gives

$$\begin{aligned} f_i^\sigma(\mathbf{x} + c^\sigma \mathbf{e}_i \Delta t, t + \Delta t) = {} & f_i^\sigma(\mathbf{x}, t) + \Delta t \partial_t f_i^\sigma + \Delta t c^\sigma e_{i\beta} \partial_{x_\beta} f_i^\sigma \\ & + \frac{(\Delta t)^2}{2} [\partial_t \partial_t f_i^\sigma + 2 c^\sigma e_{i\beta} \partial_t \partial_{x_\beta} f_i^\sigma \\ & + (c^\sigma)^2 e_{i\beta} e_{i\gamma} \partial_{x_\beta} \partial_{x_\gamma} f_i^\sigma] + O(\Delta t^3). \end{aligned} \tag{27}$$

Two time scales and one spatial scale that are involved for the change of quantities are introduced as [26]

$$\partial_t = \varepsilon \partial_{t^{(1)}} + \varepsilon^2 \partial_{t^{(2)}}, \tag{28}$$

$$\partial_{x_\beta} \to \varepsilon \partial_{x_\beta^{(1)}}. \tag{29}$$

Substituting Eqs. (17), (18), and (27)–(29) into Eq. (6), the resulting equations to $O(\varepsilon)$ and $O(\varepsilon)^2$ are given as Eqs. (C3) and (C4), which are shown in Appendix C. Multiplying each term of Eq. (C3), respectively, by ϵ_i^σ and $p e_{i,\alpha}$, and summarizing all terms over all phonon states, yields the equilibrium energy and momentum equations as

$$\partial_{t^{(1)}} E^{(\mathrm{eq})} + \partial_{x_\beta^{(1)}} Q_\beta^{(\mathrm{eq})} = 0, \tag{30}$$

and

$$\partial_{t^{(1)}} P_\alpha^{(\mathrm{eq})} + \partial_{x_\beta^{(1)}} B_{\alpha\beta}^{(\mathrm{eq})} = -\frac{1}{\varepsilon \Delta t \tau_U} P_\alpha^{(\mathrm{eq})}. \tag{31}$$

The right-hand side of Eq. (31) is a "sink" of momentum that results from the resistive U processes.

The nonequilibrium distribution functions $f_i^{\sigma(1)}$ can be expressed as (see Appendix D for the details)

$$f_i^{\sigma(1)} = \Psi_i^+ + \Psi_i^-, \tag{32}$$

where Ψ_i^+ and Ψ_i^- are given as

$$\begin{aligned} \Psi_i^+ = {} & -\Delta t \tau_C \left[w_i^\sigma \beta_0 \epsilon_i^\sigma \bar{f}_{0,i}'^{\sigma(0)} \left(\frac{M_3}{M_1} \right) \delta_{\gamma\ell} \right. \\ & \left. - w_i^\sigma \beta_0 \epsilon c^\sigma \bar{f}_{0,i}'^{\sigma(0)} e_{i\gamma} e_{i\ell} \right] \partial_{x_\gamma}^{(1)} v_\ell, \end{aligned} \tag{33}$$

$$\begin{aligned} \Psi_i^- = {} & -\Delta t \tau_C \left[w_i^\sigma \beta_0 \epsilon \bar{f}_{0,i}'^{\sigma(0)} \left(\frac{M_3}{\epsilon M_2} \right) e_{i\ell} \delta_{\ell\gamma} \right. \\ & \left. - w_i^\sigma \beta_0 \epsilon_i^\sigma c^\sigma \bar{f}_{0,i}'^{\sigma(0)} e_{i\gamma} \right] \partial_{x_\gamma}^{(1)} \theta. \end{aligned} \tag{34}$$

Using the fact the odd-numbered velocity tensors (that averages with respect to the equilibrium distribution function having an odd number of velocities) are zero, we have

$$\sum_{i,\sigma} \epsilon_i^\sigma \Psi_i^- = 0 \quad \text{and} \quad \sum_{i,\sigma} p e_{i,\alpha} \Psi_i^+ = 0. \tag{35}$$

Additional relations for Ψ_i^+ and Ψ_i^- are presented by Eqs. (D4) and (D5) as

$$\sum_{i,\sigma} \epsilon_i^\sigma \Psi_i^+ = 0 \quad \text{and} \quad \sum_{i,\sigma} p e_{i,\alpha} \Psi_i^- = 0. \tag{36}$$

Substituting Eq. (32) into Eqs. (19)–(22) yields the nonequilibrium quantities

$$E^{(\text{neq})} = \sum_{i,\sigma} \epsilon_i^\sigma f_i^{\sigma(1)} = \sum_{i,\sigma} \epsilon_i^\sigma (\Psi_i^+ + \Psi_i^-) = 0, \tag{37}$$

$$P_\alpha^{(\text{neq})} = \sum_{i,\sigma} p e_{i\alpha} f_i^{\sigma(1)} = \sum_{i,\sigma} p e_{i\alpha} (\Psi_i^+ + \Psi_i^-) = 0, \tag{38}$$

$$Q_\beta^{(\text{neq})} = \sum_{i,j,\sigma} \epsilon_i^\sigma c^\sigma e_{i\beta} f_i^{\sigma(1)} = -\Delta t \tau_C \left[\frac{-(M_3)^2}{\epsilon M_2} + M_4 \right] \delta_{\beta\gamma} \partial_{x_\gamma}^{(1)} \theta, \tag{39}$$

and

$$B_{\alpha\beta}^{(\text{neq})} = \sum_{i,\sigma} p e_{i\alpha} c^\sigma e_{i\beta} f_i^{\sigma(1)} = -p\Delta t \tau_C \left[-\frac{(M_3)^2}{\epsilon M_1} \delta_{\alpha\beta}\delta_{\gamma\ell} + M_5(\delta_{\alpha\beta}\delta_{\gamma\ell} + \delta_{\alpha\gamma}\delta_{\beta\ell} + \delta_{\alpha\ell}\delta_{\beta\gamma}) \right] \partial_{x_\gamma}^{(1)} \delta v_\ell, \tag{40}$$

where coefficients M_4 and M_5 are also given in Appendix B. Equations (37)–(40) indicate the nonequilibrium distribution functions $f_i^{\sigma(1)}$ make no contributions to quantities E and $\mathbf{P}$, but they do affect heat flux vector $\mathbf{Q}$ and momentum flux tensor $B_{\alpha\beta}$.

Substituting Eq. (32) into Eq. (C4), the energy and momentum equations to $O(\varepsilon^2)$ are obtained as the following:

$$\partial_{t^{(2)}} E^{(\text{eq})} - \frac{1}{2\varepsilon\tau_U} \partial_{x_\beta^{(1)}} Q_\beta^{(\text{eq})} + \left(1 - \frac{1}{2\tau_U}\right) \partial_{x_\beta^{(1)}} Q_\beta^{(\text{neq})} = 0, \tag{41}$$

and

$$-\frac{1}{2\varepsilon\tau_U} \partial_{t^{(1)}} P_\alpha^{(\text{eq})} + \partial_{t^{(2)}} P_\alpha^{(\text{eq})} + \left(1 - \frac{1}{2\tau_u}\right) \partial_{x_\beta^{(1)}} B_{\alpha\beta}^{(\text{neq})} = 0. \tag{42}$$

The whole conservation equations of energy and momentum are obtained as the following. [$\varepsilon\cdot$Eq. (30)$+\varepsilon^2\cdot$Eq. (41)] gives the energy equation as

$$\partial_t E^{(\text{eq})} + \left(1 - \frac{1}{2\tau_U}\right) \partial_{x_\beta} Q_\beta^{(\text{eq})} + \left(1 - \frac{1}{2\tau_U}\right) \partial_{x_\beta} \varepsilon Q_\beta^{(\text{neq})} = 0, \tag{43}$$

and [$\varepsilon\cdot$Eq. (31)$+\varepsilon^2\cdot$Eq. (42)] represents the momentum equations

$$\left(1 - \frac{1}{2\tau_u}\right) \partial_t P_\alpha^{(\text{eq})} + \partial_{x_\beta} B_{\alpha\beta}^{(\text{eq})} + \left(1 - \frac{1}{2\tau_u}\right) \partial_{x_\beta} \varepsilon B_{\alpha\beta}^{(\text{neq})} + \frac{1}{\Delta t \tau_U} P_\alpha^{(\text{eq})} = -\frac{1}{2\varepsilon\tau_U} \varepsilon^3 \partial_{t^{(2)}} P_\alpha^{(\text{eq})}. \tag{44}$$

Equations (14), (24), and (38) indicate the phonon drift velocity can be expressed as $P_\alpha = \Sigma_{i,\sigma} p e_{i,\alpha} f_i^\sigma = \Sigma_{i,\sigma} p e_{i,\alpha} f_i^{\sigma(0)} = p M_2 \delta_{\alpha\ell} v_\ell$, or

$$v_\ell = \delta_{\ell\alpha} \left[\sum_{i,\sigma} p e_{i\alpha} f_i^\sigma / p M_2 \right]. \tag{45}$$

Similarly, Eqs. (13), (23), and (37) lead to the expression of temperature θ as

$$\theta = \left(\sum_{i,\sigma} \epsilon_i^\sigma f_i^\sigma - E_0 \right) / M_1. \tag{46}$$

Once $\mathbf{v}$ and θ are obtained, substituting Eqs. (45) and (46) into Eq. (9) completes the calculation of the displaced Planck distribution functions $f_i^{\sigma(0)}$.

D. *Macroscopic equations and thermal wave equation*

Equations (43) and (44) can be expressed in terms of θ and $\mathbf{v}$ to $O(\varepsilon^2)$ as

$$\partial_t \theta = -\left(1 - \frac{1}{2\tau_U}\right) \left(\frac{M_2}{M_1}\right) \nabla \cdot \mathbf{v} + \tau_C' [-V_{\text{I}}^2 + V_{\text{II}}^2] \nabla^2 \theta, \tag{47}$$

and

$$\partial_t \mathbf{v} = -\left(1 - \frac{1}{2\tau_U}\right)^{-1} \frac{M_3}{\epsilon M_2} \nabla \theta + \left(1 - \frac{1}{2\tau_U}\right)^{-1} \times \tau_C' [V_{\text{III}}^2 \nabla^2 \mathbf{v} + (-V_{\text{I}}^2 + V_{\text{III}}^2) \nabla (\nabla \cdot \mathbf{v})] - \frac{1}{\tau_U'} \mathbf{v}. \tag{48}$$

Equations (47) and (48), obtained through the Chapman-Enskog expansion technique based on the D2Q9 lattice, are consistent with the energy and momentum equations obtained by Hardy from the linear phonon Boltzmann equation [18]. Combining Eqs. (47) and (48) through eliminating the variable $\mathbf{v}$ yields the final expression that is expressed in terms of θ as

$$\frac{\partial^2 \theta}{\partial t^2} + \frac{1}{\tau_U'} \frac{\partial \theta}{\partial t} = V_{SS}^2 \nabla^2 \theta + \tau_C' U_{SS}^2 \frac{\partial}{\partial t} \nabla^2 \theta - \tau_C'^2 C_{SS}^4 \nabla^4 \theta. \tag{49}$$

Coefficients in these expressions are summarized as

$$\tau_U' = \Delta t (\tau_U - 0.5), \tag{50}$$

$$\tau_C' = \Delta t (\tau_C - 0.5), \tag{51}$$

$$V_{\text{I}} = \left[\frac{(M_3)^2}{\epsilon M_1 M_2} \right]^{1/2}, \quad V_{\text{II}} = \left(\frac{M_4}{M_1} \right)^{1/2}, \quad V_{\text{III}} = \left(\frac{M_5}{M_2} \right)^{1/2}, \tag{52}$$

$$V_{SS} = \left[V_{\text{I}}^2 - \left(\frac{\tau_C'}{\tau_U'} \right) V_{\text{I}}^2 + \left(\frac{\tau_C'}{\tau_U'} \right) V_{\text{II}}^2 \right]^{1/2}, \tag{53}$$

TABLE I. Correspondence of parameters between Eqs. (56) and (58).

DPL-based equation	PTWE
τ_q	τ'_U
τ_T	$(U_{ss}/V_{ss})^2\tau'_C$
α	$\tau'_U V_{ss}^2$
V	V_{ss}

$$U_{SS}=\left[\left(1-\frac{1}{2\tau_U}\right)^{-1}(-V_{\mathrm{I}}^2+3V_{\mathrm{III}}^2)+(-V_{\mathrm{I}}^2+V_{\mathrm{II}}^2)\right]^{1/2}, \tag{54}$$

and

$$C_{SS}=\left[\left(1-\frac{1}{2\tau_U}\right)^{-1}(-V_{\mathrm{I}}^2+3V_{\mathrm{III}}^2)(-V_{\mathrm{I}}^2+V_{\mathrm{II}}^2)\right]^{1/2}. \tag{55}$$

Equation (49) describes the propagation of a thermal disturbance based on the phonon Boltzmann equation. Hereafter, it is named as the phonon thermal wave equation, abbreviated as PTWE, for later discussion.

III. RESULTS AND DISCUSSION

Although the particle-based phonon Boltzmann equation describes both "individual" and "collective" behaviors of phonon interactions, the PTWE, Eq. (49), is derived under the assumption of small disturbances; i.e., phonons at all states deviate slightly from the equilibrium (displaced) Planck distributions. Implicitly, it is assumed there is enough time for an equilibrium distribution to be established; i.e., the nonequilibrium state of the phonon system can be completely described by the collective variables θ and $\mathbf{v}$.

The thermal wave equation based on the DPL model, Eq. (1), is written in the following dimensionless form:

$$\frac{\partial^2\theta}{\partial t^2}+\frac{1}{\tau_q}\frac{\partial\theta}{\partial t}=\frac{\alpha}{\tau_q}\frac{\partial^2\theta}{\partial x^2}+\alpha\frac{\tau_T}{\tau_q}\frac{\partial}{\partial t}\frac{\partial^2\theta}{\partial x^2}. \tag{56}$$

Casting to the same form of Eq. (56), the PTWE is rewritten as

$$\frac{\partial^2\theta}{\partial t^2}+\frac{1}{\tau'_U}\frac{\partial\theta}{\partial t}=V_{ss}^2\frac{\partial^2\theta}{\partial x^2}+\tau'_C U_{SS}^2\frac{\partial}{\partial t}\frac{\partial^2\theta}{\partial x^2}-\tau'^2_C C_{SS}^4\frac{\partial^4\theta}{\partial x^4}. \tag{57}$$

For the purpose of comparison and discussion, terms and parameters employed in the DPL model are taken on for later discussion. By drawing an analogy between Eqs. (56) (57), Eq. (57) is reexpressed as

$$\frac{\partial^2\theta}{\partial t^2}+\frac{1}{\tau_q}\frac{\partial\theta}{\partial t}=\frac{\alpha}{\tau_q}\frac{\partial^2\theta}{\partial x^2}+\alpha\frac{\tau_T}{\tau_q}\frac{\partial}{\partial t}\frac{\partial^2\theta}{\partial x^2}-\left(\frac{C_{ss}}{U_{ss}}\right)^4\left(\tau_T\frac{\alpha}{\tau_q}\right)^2\frac{\partial^4\theta}{\partial x^4}. \tag{58}$$

Correspondence of parameters for the DPL-based equation and the PTWE are shown in Table I. Comparing Eq. (58) with Eq. (56), the third term on the right-hand side of Eq. (58), derived with respect to space to the fourth order, is the newly introduced term from the hydrodynamic approximation of the phonon Boltzmann equation. An analysis of τ_q and τ_T indicates that both equations reduce to the diffusion model employing Fourier's law as τ_q approaches zero. For finite τ_q, they both move toward the CVW equation as τ_T approaches zero. Thus, the effect of the fourth-order spatial derivative term in the PTWE is considerable when τ_q and τ_T are both finite. Besides, the second-sound mode, i.e., the propagation of temperature fluctuations as waves, emerges when N processes are the predominant mechanism. The relatively large values of τ_q to τ_T should be implemented to fulfill this requirement. Therefore, in the following illustrative examples, numerical values for τ_q and τ_T are set such that τ_T is relatively smaller than τ_q but is still finite. The detailed numerical values for parameters used in calculations are presented in Table II.

The first illustrative example concerns the propagation of a thermal wave in a single-phased medium induced by imposing a sudden impulsive volumetric heat source between $0\le x\le 0.05$ at $t=0$. An adiabatic boundary condition was imposed at $x=0$ [12]. Numerical values for parameters are given as $\tau_T=5.974\,967\times10^{-4}$, $\tau_q=1.0$, and $\alpha=9.0021\times10^{-1}$. Figure 2 shows distributions of temperature at three different times. The solid lines represent the results for the PTWE calculated by the present lattice-Boltzmann scheme and the dot points show solutions for Eq. (56). The thermal pulse propagates to the right at a speed of 0.95. As time evolves, due to the dissipation mechanism, the strength of the pulse is decreased and the width of the pulse is increased.

TABLE II. Numerical values for parameters employed in calculations.

τ_N	τ_U	τ_T	τ_q	α	$V=\sqrt{\alpha/\tau_q}$
0.8	1000.5	$3.584\,999\times10^{-4}$	1.000000047	$9.002\,119\,121\,3\times10^{-1}$	0.94879498
1	1000.5	$5.974\,967\times10^{-4}$	1.000000047	$9.003\,372\,491\,3\times10^{-1}$	0.94886103
10	1000.5	$1.118\,721\times10^{-2}$	1.000000047	$9.059\,260\,636\,8\times10^{-1}$	0.95180148
20	1000.5	$2.258\,657\times10^{-2}$	1.000000047	$9.120\,202\,416\,7\times10^{-1}$	0.95499751
25	1000.5	$2.814\,705\times10^{-2}$	1.000000047	$9.150\,227\,608\,5\times10^{-1}$	0.95656822
40	1000.5	$4.429\,822\times10^{-2}$	1.000000047	$9.238\,571\,794\,0\times10^{-1}$	0.96117489
50	1000.5	$5.464\,452\times10^{-2}$	1.000000047	$9.296\,066\,296\,4\times10^{-1}$	0.96416110
100	1000.5	$1.018\,722\times10^{-1}$	1.000000047	$9.567\,865\,613\,8\times10^{-1}$	0.978115

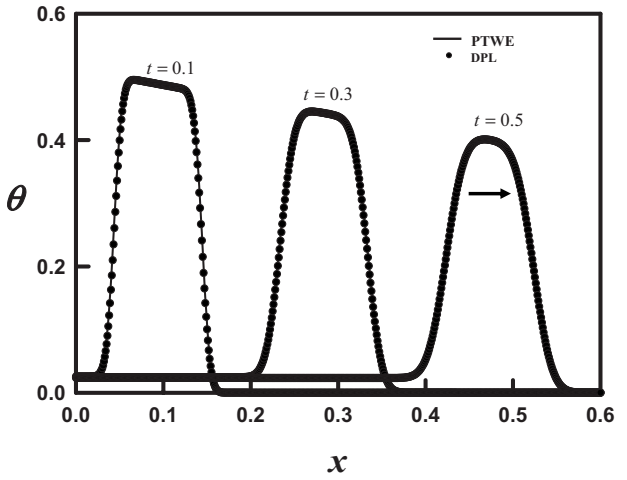

FIG. 2. Temperature distributions, subjected to a suddenly imposed pulsed volumetric heat source around $x=0$, in a single-phased medium, at times $t=0.1$, 0.3, and 0.5. The solid lines and dot points are the results based on the PTWE model and the DPL model, respectively. Numerical values for parameters are given as $\tau_T = 5.974\,967 \times 10^{-4}$, $\tau_q = 1.0$, and $\alpha = 9.0021 \times 10^{-1}$.

For this case, the macroscopic contribution from the fourth-ordered spatial derivative term of PTWE is trivial, i.e., Eq. (58) converges to Eq. (56), thus, very good agreement between the two results is observed. However, with the increase of τ_T the contribution from the fourth-ordered spatial derivative term to the PTWE becomes more important and the deviation between these two equations turns out to be significant.

Figures 3(a) and 3(b) show, respectively, the effect of τ_T on the temperature distribution-based Eqs. (58) and (56) at a particular time of $t=0.3$. Except for τ_T, all parameters are kept the same as they were for Fig. 2. As τ_q is fixed, an increase of τ_T means a reduction in the strength of N processes, which results in an increase of the pulse width and a reduction in the pulse strength. It is noted that although the corresponding second-sound speeds are set the same for these two equations, with an increase of τ_T, the positions of the peak value of thermal pulse shift toward the left of the x axis in Fig. 3(b). In Fig. 3(a), these peak positions can be kept at $x=V_{ss}t$. Depending on the relative magnitudes of τ_T and τ_q, characteristics of thermal wave within the framework of the DPL model can be discussed in three categories: $\tau_T = \tau_q$, $\tau_T > \tau_q$, and $\tau_T < \tau_q$ [9]. For $\tau_T = \tau_q$, the DPL model reduces to the diffusion model employing Fourier's law. For $\tau_T > \tau_q$, due to the heat flux vector preceding the temperature gradient in the process of heat transfer, the DPL model predicts a stronger diffusive effect than Fourier's law does. When $\tau_T < \tau_q$, the DPL model indicates the wave characteristics are in-between those of the CVW model and Fourier's. The present cases are for $\tau_q > \tau_T$, thus, as τ_T is approaching τ_q, the mode should switch from thermal wave to diffusion. This development appears exactly in Fig. 3(b). As τ_T is increased and becomes close to τ_q, the position of the peak value is shifted toward $x=0$, where the maximum temperature would occur if the Fourier law for diffusion is employed.

Figure 3(a) indicates, as τ_T increases, the PTWE does not move to the Fourier diffusion model. The fourth-ordered spatial derivative term in the PTWE prevents this reduction. According to the phonon propagating modes [20], for large values of τ_q, as τ_T is increased gradually from a small value to τ_q, the phonon interaction mode is switching from the second sound to the ballistics that is beyond the description of the PTWE. In Fig. 3(a), curve a to curve d are within the frame of PTWE. With the increase of τ_T and getting closer to τ_q, the ballistic propagating mode is observable from curve e, where the longitudinal polarized phonons and transverse polarized phonons propagate with different speeds. The propagating modes of phonons indicate that reducing from the second-sound mode to the diffusion mode can only be accomplished through the reduction of τ_q, i.e., increasing the strength of U processes. An increase of τ_T, meaning a reduction of the strength of N processes, does enhance the effect of diffusion that results in broadening the width of the thermal pulse for the present case. It, however, cannot solely lead to the switch from the second-sound mode to the diffusion mode. In the DPL model, however, the increase of τ_T not only broadens the width of the thermal pulse but also pushes

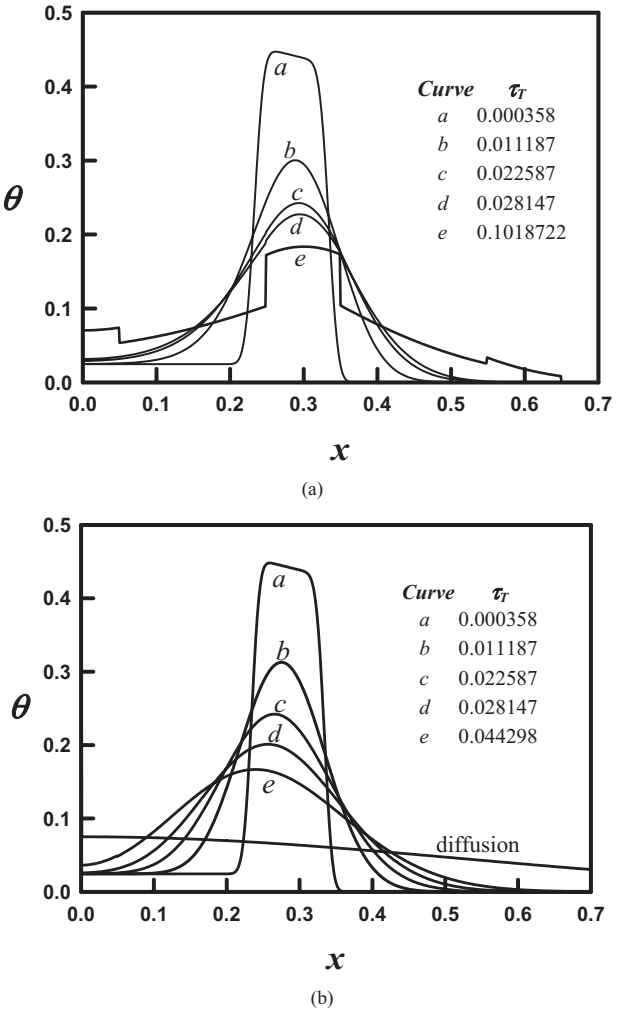

FIG. 3. Temperature distributions for different τ_T at a particular time $t=0.3$. (a) shows the results from the present lattice-Boltzmann model. (b) indicates the results based on the DPL model. Computational conditions and numerical values of parameters, except for τ_T, are set the same as they were for Fig. 2.

the wave mode toward the Fourier diffusion mode. The fundamental mechanisms of the reduction from the second-sound mode to the diffusion mode for these two models are thus different. Although it is claimed that the DPL model has the same form as the energy equation in the phonon scattering model [9], the DPL model cannot exactly represent the elementary phonon propagating modes.

The second illustrative example considers the fundamental difference in transport phenomena, both transient and steady state, in a two-layered thin film structure. Consider a thin film that is in the extent of $0 \le x \le 1$ and is composed of layer I and layer II. Layer I is in $0 \le x \le 0.5$ and layer II is in $0 \le x \le 0.5$. These two layers are connected ideally at $x=0.5$. Initially, the temperature of the whole film is uniform at $\theta=0$. At time $t=0^+$, the temperature at $x=0$ is raised to $\theta=1$, while the temperature at $x=1$ is kept at $\theta=0$. The parameters are set as $\tau_{q\mathrm{I}}=\tau_{q\mathrm{II}}=1$, $\tau_{T_\mathrm{I}}=3.585\times10^{-4}$, $\tau_{T_\mathrm{II}}=5.464\times10^{-2}$, $\alpha_\mathrm{I}=0.900$, and $\alpha_\mathrm{II}=0.9296$. Transport phenomena based on the DPL model are first discussed.

Figure 4 shows temperature distributions for Eq. (56) within the thin film at several times. The temperature disturbance is mainly confined to layer I for a time smaller than 0.5 and it reaches the layer interface around $t=0.5$. After that, as time keeps evolving, part of the energy penetrates the interface into layer II and part of the energy is reflected back to layer I. Since τ_{T_II} is larger than τ_{T_I}, the interface is able to reflect a relative minus wave back to layer I. As time evolves to $t=0.6$ and 0.8, the reflected temperature pulse in layer I moves continuously back to $x=0$ and the penetrated energy makes the temperature in layer II increase. As time reaches $t=1.0$, both the reflected wave in layer I and the penetrated wave front in layer II reach boundaries at $x=0$ and $x=1$. As time keeps increasing, the wall at $x=0$ reflects a positive wave back to layer I, and the wall at $x=1$ reflects a negative wave back to layer II that passes the "cooling" into the film. These two reflected waves meet each other at layer interface around time $t=1.55$. The waves keep being dissipated and spreading as propagation continues and become more and more unclear. At steady state the temperature distribution is very close to a straight line in the whole film. This is because for the present case the difference between α_I and α_II is very small and a discrepancy in τ_T of the two layers makes no contribution to the steady-state response. This is an expected result since Eq. (56) reduces to $\partial^2\theta/\partial x^2=0$ as $t\to\infty$. The material property τ_T thus only affects heat transfer at transient time but plays no role at all at steady state. Some transport phenomena of transmission reflection at an interface based on the DPL model were discussed in our previous work [12].

A history of temperature at the layer interface is presented in Fig. 5. The interface temperature based on the DPL model, denoted as $\theta_{\mathrm{int}}^{\mathrm{DPL}}$, shows the interface is almost undisturbed until the arrival of heat disturbance. It then increases rapidly at the duration as the front of temperature rising is passing through the interface, $t=0.5$ to 0.6, then increases slowly to the maximum value around $t=1$ at which the thermal wave arrives, $x=1$. Thus at this stage, $(0 \le t \le 1)$, the temperature increase at the interface is due to the "heating" from the wall at $x=0$. At the second stage, $(1 \le t \le 2)$, the interface temperature decreases from maximum to a minimum around

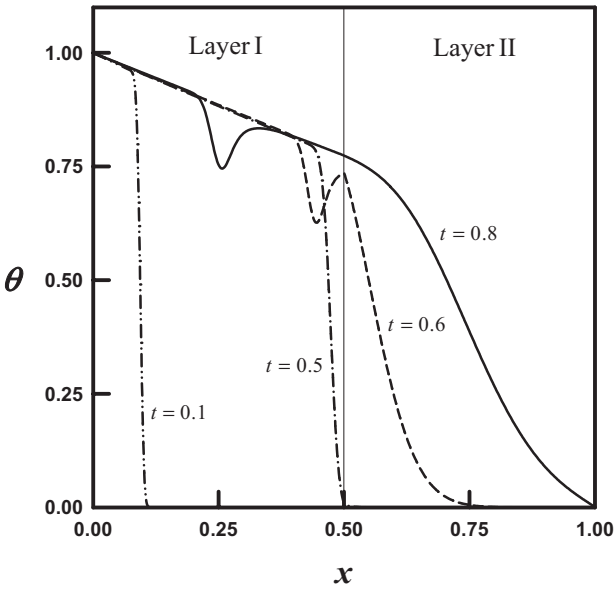

(a)

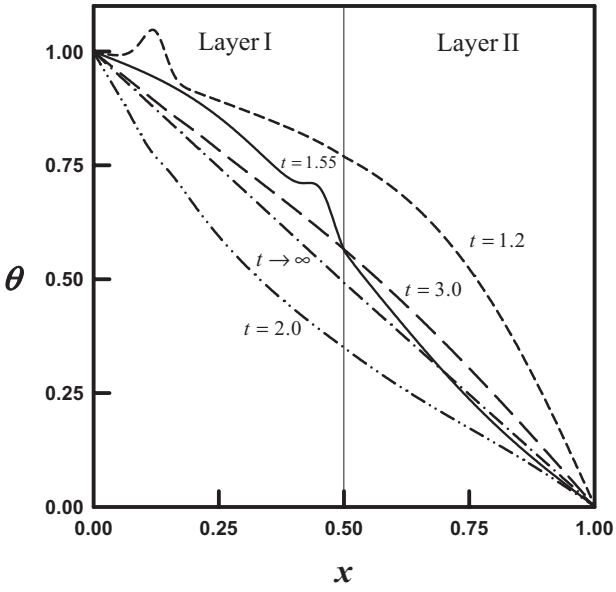

(b)

FIG. 4. Temperature distributions, based on the DPL model, at different times in a two-layered thin film structure subjected to boundary conditions $\theta=1$ and $\theta=0$ at $x=0$ and $x=1$, respectively. (a) shows the temperature distributions for times at $t=0.1$, 0.5, 0.6, and 0.8. (b) shows the temperature distributions for times at $t=1.2$, 1.55, 2.0, and 3.0 as well as $t\to\infty$.

$t=2$. This cooling is due to the reflected wave from the cold wall at $x=1$. It is noted there is a little "rebound," circled in Fig. 5, occurring during $t=1.5-1.6$. This is a result from the positive wave reflecting from the heating wall that is passing through the interface at this duration (see the temperature distribution curve at $t=1.55$ in Fig. 4). At the third stage, $2 \le t \le 3$, interface temperature increases and then decreases at the fourth stage, $3 \le t \le 4$. This oscillation maintains the same period until it is indistinguishable. The rebound at the

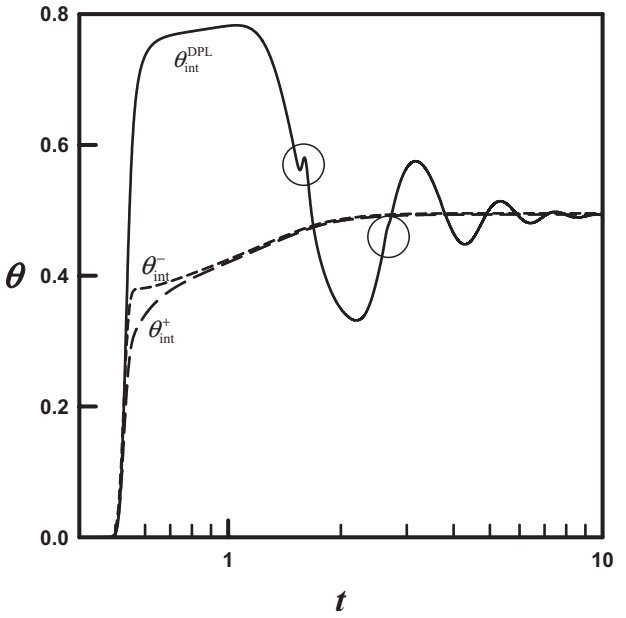

FIG. 5. History of temperatures at the layer interface. θ_{int}^{DPL} is the temperature based on the DPL model while θ_{int}^{-} and θ_{int}^{+} are temperatures from the PTWE and represent the interface temperatures from layer I and layer II, respectively. The circled regions indicate the times occurring with observable temperature rebounds. Boundary conditions are the same as they were in Fig. 4.

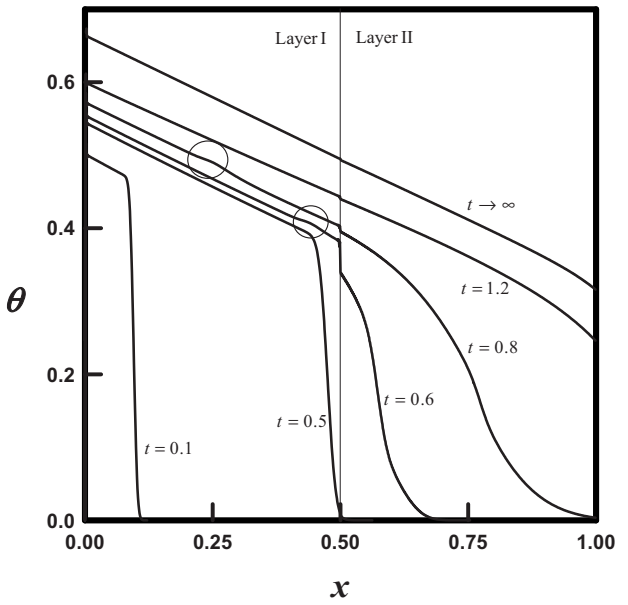

FIG. 6. Temperature distributions, based on the PTWE, in a two-layered thin film structure for times at $t=0.1$, 0.5, 0.6, 0.8, and 1.2 as well as $t\to\infty$. Two slight "swellings," circled on the curves at $t=0.6$ and $t=0.8$, show the observable reflected positive thermal waves from the layer interface. Boundary conditions are the same as they were in Fig. 4.

second stage still appears at the third stage but becomes undetectable by the fourth stage.

Results for PTWE based on the present lattice-Boltzmann scheme, however, show considerably different trends from those based on the DPL model. Figure 6 shows temperature distributions within the film at several times. A temperature jump occurring at $x=0$ can be clearly observed. As time evolves, temperature at $x=0^+$ first increases fast, then, with the decrease of the temperature difference between the film and the boundary, the rate of the increase is gradually reduced until the steady state is reached. This jump at boundary, due to the fact that distribution functions for phonons are different at boundary and within the film, is naturally formed using the present lattice-Boltzmann scheme. The degree of the jump depends on the strength of N processes. For stronger N processes collisions among phonons relax the distribution function more toward the displaced Planck distribution. Since the wall is assumed at the Planck distribution, the difference of drift velocity makes the temperature jump at the boundary. On the contrary, for stronger U processes, the more frequent phonon resistive scattering makes the distribution of phonons closer to the "driftless" Planck distribution, which results in a more continuous temperature distribution at the boundary. For the Fourier model, phonon interactions are only through the U processes; no temperature jump would occur for an ideal boundary.

Figure 6 further shows as the wave front of the temperature pulse arrives at the layer interface, a second temperature jump occurs there. A third jump then appears as the penetration wave in layer II reaches the film's other boundary at $x=1$. Unlike the DPL model that reflects a relative negative wave, the interface here reflects a relative positive wave. Although its magnitude is small, this "swelling" is still detectable (see the circled regions on the curves for times at $t=0.6$ and 0.8). The opposite sign in the reflected wave from the layer interface is more evidence concerning the fundamental differences of wave characteristics between the two considered models. Reflecting a negative wave from the layer interface is usually unfavorable because a thermodynamic state with negative temperature, which is physically unreal, is achievable at a low temperature due to the negative wave. A temperature jump at the layer interface as a function of time is also presented in Fig. 5. θ_{int}^{-} and θ_{int}^{+} represent temperatures of the lattice points that are closest to the layer interface and are sited, respectively, in layer I and layer II. The jump commences as the thermal front of temperature rising arrives at the interface, increases quickly during the wave front penetrating the interface, and decreases gradually after the penetration. Compared to the trend of θ_{int}^{DPL}, θ_{int}^{-} and θ_{int}^{+} have no observable oscillations but there exists a finite temperature difference at steady state. The temperature distribution at steady state, shown in Fig. 6, is not a straight line. This can be further confirmed from Eq. (58). As $t\to\infty$, Eq. (58) is reduced to

$$\frac{\partial^2\theta}{\partial x^2} - (C_{ss}/U_{ss})^4 \tau_T^2 \alpha/\tau_q \frac{\partial^4\theta}{\partial x^4} = 0,$$

or simply,

$$\theta - (C_{ss}/U_{ss})^4 \tau_T^2 \alpha/\tau_q \frac{\partial^2\theta}{\partial x^2} = \text{const}.$$

This expression shows that the material property τ_T affects not just the transient behavior but also the steady-state re-

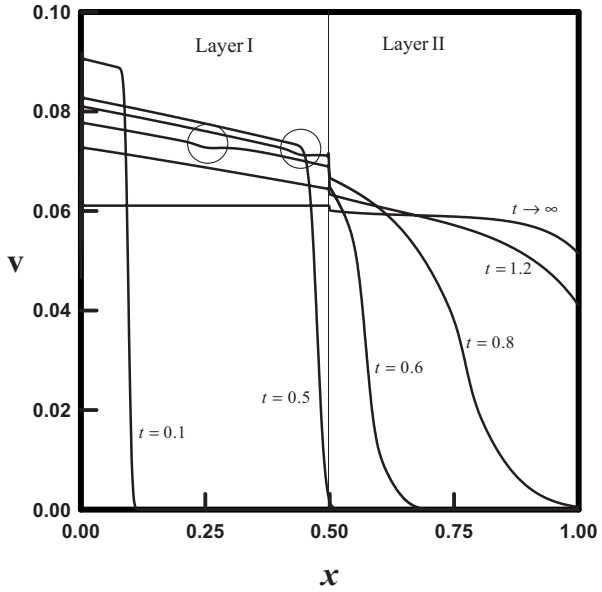

FIG. 7. Distributions of the phonon drift velocity, based on the PTWE, in a two-layered thin film structure for times at $t=0.1$, 0.5, 0.6, 0.8, and 1.2 as well as $t\rightarrow\infty$. Two slight "dents," circled on the curves at $t=0.6$ and $t=0.8$, show the observable reflected negative velocity disturbances from the layer interface that correspond to the circled reflected thermal waves in Fig. 6. Boundary conditions are the same as they were in Fig. 4.

sponse. This provides another fundamental difference between the two considered models.

Distributions of drift velocity and heat flux within the film at times corresponding to Fig. 6 are shown in Figs. 7 and 8. The drift velocity first is continuous in layer I, then a jump at the layer interface is formed as the front of temperature rising passes through the interface. Discontinuity in the drift velocity at boundaries and at the interface leads to the shift of phonon distribution functions that results in a temperature jump. The circled regions on the curves for times at $t=0.6$ and 0.8 in Fig. 7 show that the layer interface reflects a detectable "minus" velocity disturbance in the drift velocity that is responsible for the slight "swelling" in Fig. 6. Although temperature is discontinuous at the interface, Fig. 8, however, shows a continuous heat flux is always satisfied. Compared to the continuity of temperature, the continuity of heat flux is the primary condition to fulfill for the conservation of energy principle at the interface. With the advantage of a distribution-function-based Boltzmann equation, a temperature jump at the boundary and at the layer interface, can be calculated naturally and straightforwardly using the lattice-Boltzmann scheme, providing material properties in the two layers and the boundary conditions are prescribed.

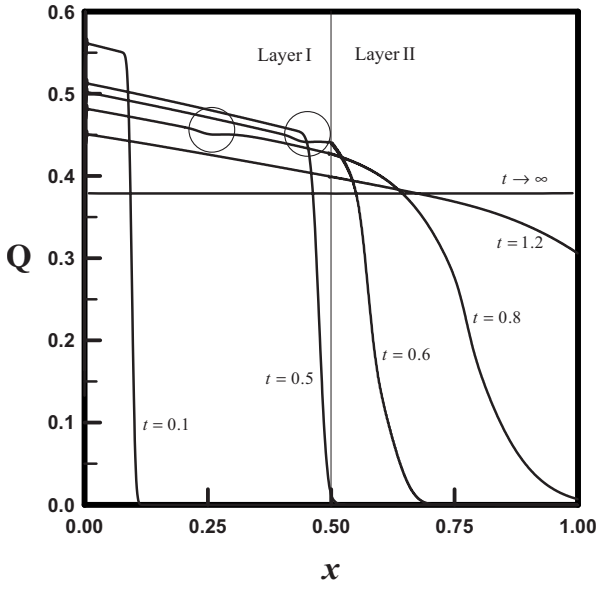

FIG. 8. Distributions of heat flux, based on the PTWE, in a two-layered thin film structure for times at $t=0.1$, 0.5, 0.6, 0.8, and 1.2 as well as $t\rightarrow\infty$. The circled regions placed on the curves at $t=0.6$ and $t=0.8$ show the slight reduction in heat flux due to the reflected thermal wave. Boundary conditions are the same as they were in Fig. 4.

IV. CONCLUSIONS

In this study, a hydrodynamic approximation to a phonon Boltzmann equation is accomplished through the lattice-Boltzmann method. Both the thermal excited transverse and longitudinal phonons that interact through normal (N) and umklapp (U) processes are considered. The collision term in the Boltzmann equation is approximated by the relaxation time model with two constants τ_U and τ_N that represent the times required for U and N processes to relax the distributions of phonons to their corresponding equilibrium distribution functions—the Planck distribution and the displaced Planck distribution, respectively. Through the technique of Chapman-Enskog expansion, a macroscopic thermal wave equation that is valid for the phonon collective, second-sound mode is obtained.

Compared to the thermal wave equation based on the dual-phase-lag (DPL) model, mathematically the macroscopic phonon thermal wave equation (PTWE) has an additional term for a fourth-ordered derivative in space. The fundamental difference of wave characteristics between the two models is discussed through two illustrative examples. One illustrates a propagating thermal pulse in a single-phased medium; the other demonstrates both transient and steady-state transport phenomena in a two-layered thin film structure subjected to different fixed temperatures at boundaries. Besides, to fulfill the requirement for the second-sound mode, numerical values for τ_q and τ_T are set such that τ_T is relatively smaller than τ_q but is still noticeable.

The thermal wave equation based on the DPL model is reduced to the diffusion model based on Fourier's law through either reducing τ_q to zero, or τ_T approaches τ_q at finite τ_q. Phonon propagating modes, however, indicate that switching from the second-sound mode to the diffusion mode can only be accomplished through reducing τ_q to zero. Thus, a reduction from the wave mode to the diffusion mode through the later path claimed in the DPL model, τ_T approaching τ_q, finds no compatible microscopic propagating modes. That is, missing of the fourth-ordered spatial derivative term in the DPL model fundamentally leads to improper

direction in mode reduction from the thermal wave to diffusion.

The DPL mode shows, for a two-layered structure in which $\tau_{T_{\mathrm{I}}} > \tau_{T_{\mathrm{II}}}$, the layer interface reflects a relative minus wave as an increasing temperature front is coming and the interface temperature oscillates periodically with damping until steady state. The steady-state response based on the DPL model is exactly the same as that of the diffusion model. A difference in τ_T thus only affects the process in transient. Furthermore, for an ideal contact, temperature is always continuous at the interface; thermal resistance at the interface due to material difference is unclear. Unlike the DPL model, the solution of PTWE shows the interface reflects a positive wave and τ_T affects both the process of transient as well as the response at steady state. With its advantage of description phenomena in microscopic scale, temperature jumps at the boundary and the interface can be calculated naturally and straightforwardly by the present lattice-Boltzmann method once material properties and boundary conditions are set.

ACKNOWLEDGMENTS

Support for this work by the National Science Council of the Republic of China under Grant No. NSC95-2221-E-194-052 is gratefully acknowledged.

APPENDIX A

The velocity space is discretized by introducing a finite set of velocities $\mathbf{c}_i^\sigma$, and the corresponding distribution function is discretized as $f_i^\sigma(\mathbf{x},t)$. The discrete phonon Boltzmann equation that corresponds to Eq. (4) is given as

$$\frac{\partial f_i^\sigma}{\partial t} + \mathbf{c}_i^\sigma \nabla f_i^\sigma = -\frac{1}{\tau_N \varepsilon}(f_i^\sigma - f_i^{\sigma(0)}) - \frac{1}{\tau_U \varepsilon}(f_i^\sigma - f_{0,i}^{\sigma(0)}). \tag{A1}$$

The dimensionless parameters are introduced in Sec. II A. A discretization of Eq. (A1) is given by

$$\begin{aligned}
&\frac{f_i^\sigma(\mathbf{x},t+\Delta t) - f_i^\sigma(\mathbf{x},t)}{\Delta t} + c_{ix}^\sigma \frac{f_i^\sigma(\mathbf{x}+\Delta x,t+\Delta t) - f_i^\sigma(\mathbf{x},t+\Delta t)}{\Delta x} \\
&\quad + c_{iy}^\sigma \frac{f_i^\sigma(\mathbf{x}+\Delta y,t+\Delta t) - f_i^\sigma(x,t+\Delta t)}{\Delta y} \\
&= -\frac{1}{\tau_N \varepsilon}(f_i^\sigma - f_i^{\sigma(0)}) - \frac{1}{\tau_U \varepsilon}(f_i^\sigma - f_{0,i}^{\sigma(0)}),
\end{aligned} \tag{A2}$$

where $\Delta t = \Delta \hat{t}\hat{U}/\hat{L}$. Lagrangian behavior is then obtained by the selection of the lattice spacing as $\Delta x^\sigma/\Delta t = c_{ix}^\sigma$, which yields

$$\begin{aligned}
&\frac{f_i^\sigma(\mathbf{x},t+\Delta t) - f_i^\sigma(\mathbf{x},t)}{\Delta t} + \frac{f_i^\sigma(\mathbf{x}+c^\sigma \mathbf{e}_i \Delta t,t+\Delta t) - f_i^\sigma(\mathbf{x},t+\Delta t)}{\Delta t} \\
&= \frac{f_i^\sigma(\mathbf{x}+c^\sigma \mathbf{e}_i \Delta t,t+\Delta t) - f_i^\sigma(\mathbf{x},t)}{\Delta t} \\
&= -\frac{1}{\tau_N \varepsilon}(f_i^\sigma - f_i^{\sigma(0)}) - \frac{1}{\tau_U \varepsilon}(f_i^\sigma - f_{0,i}^{\sigma(0)}).
\end{aligned} \tag{A3}$$

Choosing $\Delta t = t_c$, multiplying Eq. (A4) by Δt, leads to the lattice phonon Boltzmann equation given by Eq. (5).

APPENDIX B

Definitions for parameters that are frequently used in formulations in this study are as follows:

$$M_1 = -\frac{1}{2}\left[\sum_\sigma 4 w_{1\to 4}^\sigma \beta_0 (\epsilon_{1\to 4}^\sigma)^2 \bar{f}'^{\sigma(0)}_{0,1\to 4} + 4 w_{5\to 8}^\sigma \beta_0 (\epsilon_{5\to 8}^\sigma)^2 \bar{f}'^{\sigma(0)}_{0,5\to 8}\right], \tag{B1}$$

$$M_2 = -\frac{1}{2}\left[\sum_\sigma 2 w_{1\to 4}^\sigma \beta_0 \epsilon \bar{f}'^{\sigma(0)}_{0,1\to 4} + 4 w_{5\to 8}^\sigma \beta_0 \epsilon \bar{f}'^{\sigma(0)}_{0,5\to 8}\right], \tag{B2}$$

$$M_3 = -\frac{1}{2}\left[\sum_\sigma 2 w_{1-4}^\sigma \beta_0 \epsilon \epsilon_{1\to 4}^\sigma c^\sigma \bar{f}'^{\sigma(0)}_{0,1\to 4} + 4 w_{5\to 8}^\sigma \beta_0 \epsilon \epsilon_{5\to 8}^\sigma c^\sigma \bar{f}'^{\sigma(0)}_{0,5\to 8}\right], \tag{B3}$$

$$M_4 = -\frac{1}{2}\left[\sum_\sigma 2 w_{1\to 4}^\sigma (\beta_0 \epsilon_{1\to 4}^\sigma c^\sigma)^2 \bar{f}'^{\sigma(0)}_{0,1\to 4} + 4 w_{5\to 8}^\sigma (\beta_0 \epsilon_{1\to 4}^\sigma c^\sigma)^2 \bar{f}'^{\sigma(0)}_{0,1\to 4}\right], \tag{B4}$$

$$M_5 = -\frac{1}{2}\left[\sum_\sigma 4 w_{5\to 8}^\sigma \beta_0 \epsilon (c^\sigma)^2 \bar{f}'^{\sigma(0)}_{0,5\to 8}\right]. \tag{B5}$$

APPENDIX C

Substituting Eqs. (17), (18), and (27)–(29) into Eq. (6) yields

$$\begin{aligned}
0 &= \varepsilon \Delta t[\partial_{t^{(1)}} f_i^{\sigma(0)} + c^\sigma e_{i,\beta} \partial_{x_\beta^{(1)}} f_i^{\sigma(0)}] + \varepsilon^2 \Delta t[\partial_{t^{(1)}} f_i^{\sigma(1)} + \partial_{t^{(2)}} f_i^{\sigma(0)} \\
&\quad + c^\sigma e_{i,\beta} \partial_{x_\beta^{(1)}} f_i^{\sigma(1)}] + \varepsilon^2 \frac{(\Delta t)^2}{2}[\partial \partial_{t^{(1)}} \partial_{t^{(1)}} f_i^{\sigma(0)} \\
&\quad + 2 c^\sigma e_{i,\beta} \partial_t^{(1)} \partial_{x_\beta}^{(1)} f_i^{\sigma(0)} + (c^\sigma)^2 e_{i,\beta} e_{i,\gamma} \partial_{x_\beta^{(1)}} \partial_{x_\gamma^{(1)}} f_i^{\sigma(0)}] \\
&\quad + \frac{1}{\tau_C}(\varepsilon f_i^{\sigma(1)} + \varepsilon^2 f_i^{\sigma(2)}) + \frac{1}{\tau_U}(f_i^{\sigma(0)} - f_{0,i}^{\sigma(0)} - \varepsilon f_{0,i}^{\sigma(1)}) \\
&\quad + O(\Delta t^3) + O(\varepsilon^3).
\end{aligned} \tag{C1}$$

The terms in Eq. (C1) are regrouped according to the power of ε. $O(\varepsilon^0)$ gives

$$0 = f_i^{\sigma(0)} - f_i^{\sigma(0)}. \tag{C2}$$

$O(\varepsilon^1)$ shows

$$0 = \partial_{t^{(1)}} f_i^{\sigma(0)} + c^\sigma e_{i,\beta} \partial_{x_\beta^{(1)}} f_i^{\sigma(0)} + \frac{1}{\Delta t \tau_C} f_i^{\sigma(1)} - \frac{1}{\Delta t \tau_U} f_{0,i}^{\sigma(1)}. \tag{C3}$$

$O(\varepsilon^2)$ is

$$\begin{aligned} 0 = {} & \partial_{t^{(1)}} f_i^{\sigma(1)} + \partial_{t^{(2)}} f_i^{\sigma(0)} + c^\sigma e_{i,\beta} \partial_{x_\beta^{(1)}} f_i^{\sigma(1)} + \frac{\Delta t}{2} \partial_{t^{(1)}} \partial_{t^{(1)}} f_i^{\sigma(0)} \\ & + \Delta t c^\sigma e_{i,\beta} \partial_{t^{(1)}} \partial_{x_\beta^{(1)}} f_i^{\sigma(0)} + \frac{\Delta t}{2} (c^\sigma)^2 e_{i,\beta} e_{i,\gamma} \partial_{x_\beta^{(1)}} \partial_{x_\gamma^{(1)}} f_i^{\sigma(0)} \\ & + \frac{1}{\Delta t \tau_C} f_i^{\sigma(2)}. \end{aligned} \tag{C4}$$

APPENDIX D

From Eq. (C3), $f_i^{\sigma(1)}$ can be expressed as

$$f_i^{\sigma(1)} = -\Delta t \tau_C \partial_{t^{(1)}} f_i^{\sigma(0)} - \Delta t \tau_C c^\sigma e_{i,\beta} \partial_{x_\beta^{(1)}} f_i^{\sigma(0)} + \frac{\tau_C}{\tau_U} f_{0,i}^{\sigma(1)}. \tag{D1}$$

Expressing $f_i^{\sigma(1)}$ in terms of θ and $\mathbf{v}$ gives

$$\begin{aligned} f_i^{\sigma(1)} = {} & \Delta t \tau_C w_i^\sigma \beta_0 \epsilon_i^\sigma \bar{f}_{0,i}'^{\sigma(0)} \partial_{t^{(1)}} \theta + \Delta t \tau_C w_i^\sigma \beta_0 \varepsilon \bar{f}_{0,i}'^{\sigma(0)} e_{i,\ell} \partial_{t^{(1)}} v_\ell \\ & + \Delta t \tau_C w_i^\sigma c^\sigma \beta_0 \epsilon_i^\sigma \bar{f}_{0,i}'^{\sigma(0)} e_{i,\gamma} \partial_{x_\gamma^{(1)}} \theta \\ & + \Delta t \tau_C w_i^\sigma c^\sigma \beta_0 \epsilon \bar{f}_{0,i}'^{\sigma(0)} e_{i,\gamma} e_{i,\ell} \partial_{x_\gamma^{(1)}} v_\ell \\ & + \frac{\tau_C}{\varepsilon \tau_U} w_i^\sigma \beta_0 \epsilon \bar{f}_{0,i}'^{\sigma(0)} e_{i,\ell} v_\ell. \end{aligned} \tag{D2}$$

To express the effect of spatially inhomogeneous terms, substituting Eqs. (30) and (31) into Eq. (D2) to take off terms, including a derivative with respect to time, yields

$$\begin{aligned} f_i^{\sigma(1)} = {} & -\Delta t \tau_C w_i^\sigma \beta_0 \epsilon_i^\sigma \bar{f}_{0,i}'^{\sigma(0)} \left(\frac{M_3}{M_1} \right) \delta_{\gamma\ell} \partial_{x_\gamma^{(1)}} v_\ell \\ & - \Delta t \tau_C w_i^\sigma \beta_0 \epsilon \bar{f}_{0,i}'^{\sigma(0)} e_{i\ell} \left[\left(\frac{M_3}{b M_2} \right) \delta_{\ell\gamma} \partial_{x_\gamma^{(1)}} \theta + \frac{1}{\varepsilon \Delta t \tau_U} v_\ell \right] \\ & + \Delta t \tau_C w_i^\sigma c^\sigma \beta_0 \epsilon_i^\sigma \bar{f}_{0,i}'^{\sigma(0)} e_{i\gamma} \partial_{x_\gamma^{(1)}} \theta \\ & + \Delta t \tau_C w_i^\sigma c^\sigma \beta_0 \epsilon \bar{f}_{0,i}'^{\sigma(0)} e_{i\gamma} e_{i\ell} \partial_{x_\gamma^{(1)}} v_\ell \\ & + \frac{\tau_C}{\varepsilon \tau_U} w_i^\sigma \beta_0 \epsilon \bar{f}_{0,i}'^{\sigma(0)} e_{i\ell} v_\ell. \end{aligned} \tag{D3}$$

Let $f_i^{\sigma(1)} = \Psi_i^+ + \Psi_i^-$, where

$$\begin{aligned} \Psi_i^+ = {} & -\Delta t \tau_C \left[w_i^\sigma \beta_0 \epsilon_i^\sigma \bar{f}_{0,i}'^{\sigma(0)} \left(\frac{M_3}{M_1} \right) \delta_{\gamma\ell} \right. \\ & \left. - w_i^\sigma \beta_0 \epsilon c^\sigma \bar{f}_{0,i}'^{\sigma(0)} e_{i\gamma} e_{i\ell} \right] \partial_{x_\gamma^{(1)}} v_\ell, \end{aligned} \tag{33}$$

$$\begin{aligned} \Psi_i^- = {} & -\Delta t \tau_C \left[w_i^\sigma \beta_0 \epsilon \bar{f}_{0,i}'^{\sigma(0)} \left(\frac{M_3}{\epsilon M_2} \right) e_{i\ell} \delta_{\ell\gamma} \right. \\ & \left. - w_i^\sigma \beta_0 \epsilon_i^\sigma c^\sigma \bar{f}_{0,i}'^{\sigma(0)} e_{i\gamma} \right] \partial_{x_\gamma^{(1)}} \theta. \end{aligned} \tag{34}$$

It can be shown that

$$\begin{aligned} \sum_{i\sigma} \epsilon_i^\sigma \Psi_i^+ = {} & -\Delta t \tau_C \sum_{i\sigma} \left[w_i^\sigma \beta_0 (\epsilon_i^\sigma)^2 \bar{f}_{0,i}'^{\sigma(0)} \left(\frac{M_3}{M_1} \right) \delta_{\gamma\ell} \right. \\ & \left. - w_i^\sigma \beta_0 \epsilon \epsilon_i^\sigma c^\sigma \bar{f}_{0,i}'^{\sigma(0)} e_{i\gamma} e_{i\ell} \right] \partial_{x_\gamma^{(1)}} v_\ell \\ = {} & -\Delta t \tau_C \left[-M_1 \left(\frac{M_3}{M_1} \right) \delta_{\gamma\ell} + M_3 \delta_{\gamma\ell} \right] \partial_{x_\gamma^{(1)}} \delta v_\ell = 0, \end{aligned} \tag{D4}$$

and

$$\begin{aligned} \sum_{i\sigma} p e_{i\alpha} \Psi_i^- = {} & -\Delta t \tau_C p \left[\sum_{i\sigma} w_i^\sigma \beta_0 \epsilon \bar{f}_{0,i}'^{\sigma(0)} \left(\frac{M_3}{\epsilon M_2} \right) e_{i\alpha} e_{i\ell} \delta_{\ell\gamma} \right. \\ & \left. - \sum_{i\sigma} w_i^\sigma \beta_0 \epsilon_i^\sigma c^\sigma \bar{f}_{0,i}'^{\sigma(0)} e_{i\alpha} e_{i\gamma} \right] \partial_{x_\gamma^{(1)}} \delta\alpha \\ = {} & -\Delta t \tau_C p \left[-M_2 \left(\frac{M_3}{\epsilon M_2} \right) \delta_{\alpha\ell} \delta_{\ell\gamma} \right. \\ & \left. + \left(\frac{M_3}{\epsilon} \right) \delta_{\alpha\gamma} \right] \partial_{x_\gamma^{(1)}} \delta\alpha \\ = {} & -\Delta t \tau_C p \left[-\left(\frac{M_3}{\epsilon} \right) \delta_{\alpha\gamma} + \left(\frac{M_3}{\epsilon} \right) \delta_{\alpha\gamma} \right] \partial_{x_\gamma^{(1)}} \delta\alpha = 0. \end{aligned} \tag{D5}$$

APPENDIX E: DERIVATION OF THE WEIGHTING FACTOR w_i^σ

Based on the D2Q9 lattice, tensors of rank two and rank four that appear in the formulation, appear as

$$\sum_i A_i^\sigma w_i^\sigma e_{i,\alpha} e_{i,\beta} = (2A_{1-4}^\sigma w_{1-4}^\sigma + 4A_{5-8}^\sigma w_{5-8}^\sigma) \delta_{\alpha\beta}, \tag{E1}$$

and

$$\begin{aligned} & \sum_i A_i^\sigma w_i^\sigma e_{i,\alpha} e_{i,\beta} e_{i,\gamma} e_{i,\delta} \\ & = 4A_{5-8}^\sigma w_{5-8}^\sigma (\delta_{\alpha\beta}\delta_{\gamma\delta} + \delta_{\alpha\gamma}\delta_{\beta\delta} + \delta_{\alpha\delta}\delta_{\beta\gamma}) + (2A_{1-4}^\sigma w_{1-4}^\sigma \\ & - 8A_{5-8}^\sigma w_{5-8}^\sigma) \delta_{\alpha\beta\gamma\delta}, \end{aligned} \tag{E2}$$

where

$$A_{1-4}^\sigma = A_1^\sigma = A_2^\sigma = A_3^\sigma = A_4^\sigma,$$

$$A_{5-8}^\sigma = A_5^\sigma = A_6^\sigma = A_7^\sigma = A_8^\sigma,$$

$$w_{1-4}^\sigma = w_1^\sigma = w_2^\sigma = w_3^\sigma = w_4^\sigma,$$

and

$$w_{5-8}^{\sigma} = w_5^{\sigma} = w_6^{\sigma} = w_7^{\sigma} = w_8^{\sigma}.$$

Equation (E2) is isotropic. Based on the D2Q9 lattice, the condition for Eq. (E2) to be isotropic is $2A_{1-4}^{\sigma} w_{1-4}^{\sigma} - 8A_{5-8}^{\sigma} w_{5-8}^{\sigma} = 0$. This leads to $w_{1-4}^{\sigma}/w_{5-8}^{\sigma} = 4A_{5-8}^{\sigma}/A_{1-4}^{\sigma}$. Other criteria for the weighting factors is $4(w_{1-4}^{\sigma} + w_{5-8}^{\sigma}) = 1$. Combining these two expressions yields the general form for the weighting factors as follows:

$$w_{1-4}^{\sigma} = 1/(4 + A_{1-4}^{\sigma}/A_{5-8}^{\sigma}), \tag{E3}$$

and

$$w_{5-8}^{\sigma} = 1/[4(4A_{5-8}^{\sigma}/A_{1-4}^{\sigma} + 1)]. \tag{E4}$$

In the derivation of Eq. (40), it can be shown that

$$A_{1-4}^{\sigma} = \beta_0 \epsilon (c^{\sigma})^2 \overline{f}'^{\sigma(0)}_{0,1-4}, \tag{E5}$$

and

$$A_{5-8}^{\sigma} = \beta_0 \epsilon (c^{\sigma})^2 \overline{f}'^{\sigma(0)}_{0,5-8}. \tag{E6}$$

[1] J. I. Frankel, B. Vick, and M. N. Ozisik, Int. J. Heat Mass Transfer **30**, 1293 (1987).
[2] C. Cattaneo, Compt. Rend. **247**, 431 (1958).
[3] P. Venotte, Compt. Rend. **252**, 2190 (1961).
[4] D. D. Joseph and L. Preziosi, Rev. Mod. Phys. **61**, 41 (1989).
[5] D. D. Joseph and L. Preziosi, Rev. Mod. Phys. **62**, 375 (1990).
[6] M. N. Ozisik and D. Y. Tzou, J. Heat Transfer **116**, 526 (1994).
[7] Y. Taitel, Int. J. Heat Mass Transfer **15**, 369 (1972).
[8] C. Körner and H. W. Bergmann, Appl. Phys. A: Mater. Sci. Process. **67**, 397 (1998).
[9] D. Y. Tzou, *Macro-to-Microscale Heat Transfer: The Lagging Behavior* (Taylor & Francis, Washington, D.C., 1996).
[10] D. Y. Tzou, J. Heat Transfer **117**, 8 (1995).
[11] D. Y. Tzou, Int. J. Heat Mass Transfer **38**, 3231 (1995).
[12] J. R. Ho, C. P. Kuo, and W. S. Jiaung, Int. J. Heat Mass Transfer **46**, 55 (2003).
[13] J. Callaway, Phys. Rev. **113**, 1046 (1959).
[14] E. W. Prohofsky and J. A. Krumhansl, Phys. Rev. **133**, A1403 (1964).
[15] R. A. Guyer and J. A. Krumhansl, Phys. Rev. **148**, 766 (1966).
[16] R. A. Guyer, Phys. Rev. **148**, 778 (1966).
[17] R. J. Hardy, Phys. Rev. B **2**, 1193 (1970).
[18] R. J. Hardy and D. L. Albers, Phys. Rev. B **10**, 3546 (1974).
[19] *Dynamical Properties of Solids*, edited by G. H. Horton and A. A. Maradudin (North-Holland Publishing, Amsterdam, 1975), pp. 205–284.
[20] *Nonequilibrium Phonons in Nonmetallic Crystals*, edited by W. Eisenmenger and A. A. Kaplyanskii (North-Holland Publishing, Amsterdam, 1986), Chap. 3.
[21] R. A. Guyer, Phys. Rev. E **50**, 4596 (1994).
[22] R. A. Escobar, S. S. Ghai, M. S. Jhon, and C. H. Amon, Int. J. Heat Mass Transfer **49**, 97 (2006).
[23] C. H. Amon, S. S. Chai, W. T. Kim, and M. S. Jhon, Physica A **362**, 36 (2006).
[24] R. A. Escobar, B. Smith, and C. H. Amon, J. Electron. Packag. **128**, 115 (2006).
[25] J. M. Buick and C. A. Greated, Phys. Rev. E **61**, 5307 (2000).
[26] D. Wolf-Gladrow, *Lattice-Gas Cellular Automata and Lattice Boltzmann Models: An Introduction* (Springer-Verlag, Berlin, Heidelberg, 2000).